# A probabilistic functional parcellation of human occipito-temporal cortex

Mona Rosenke[1*], Rick van Hoof[2*], Job van den Hurk[2,3], Rainer Goebel[2]

[1] Department of Psychology. Stanford University, Stanford. CA. USA

[2] Department of Cognitive Neuroscience, Faculty of Psychology and Neuroscience, Maastricht University, Maastricht, The Netherlands

[3] Scannexus MRI Center, Maastricht, The Netherlands

*authors contributed equally

**Corresponding Author:**

Rainer Goebel, Department of Cognitive Neuroscience, Faculty of Psychology and Neuroscience, Maastricht, The Netherlands, r.goebel@maastrichtuniversity.nl

**Abstract**

Ventral visual cortex can be divided into a variety of retinotopically as well as category-specific regions. These brain areas have been the focus of a large body of functional MRI research, significantly expanding our understanding of high-level visual processing. As studying these regions requires accurate localization of their cortical location, it is usually necessary to perform functional localizer runs on an individual subject level. These runs are costly in terms of scanning time and a participant's capacity level. Moreover, certain patient populations are unable to undergo such localizers, for instance the congenitally blind. In the current paper, we aimed to overcome these challenges by developing a functional atlas based on localizer- and visual field mapping data acquired in 20 healthy subjects. Single subject functional maps were aligned to both volume and surface group space, after which a probabilistic functional group atlas was created. We subsequently quantified the inter-subject variability of category-selective regions in visual cortex and the specificity of each atlas region – to our knowledge the first such analyses. Additionally, we validated our atlas against existing atlases of retinotopic as well as category-specific regions. The resulting functional atlas is made publicly available for a variety of software packages (https://share.brainvoyager.com/index.php/s/m2E9oZTGWwXodRk).

**Keywords:** visual cortex, human brain atlas, object recognition, retinotopy, cortex-based alignment

Human visual cortex can be divided into dozens of visual field maps (Arcaro et al., 2009; Wandell et al., 2005; Wandell and Winawer, 2011; Wang et al., 2014), as well as category-selective regions, each showing recognition expertise for specific visual categories, divided into three main processing streams (Goodale et al., 1991; Mishkin et al., 1983; Grill-Spector & Weiner, 2014). While the dorsal stream consists mainly of visual field maps, the lateral and ventral visual streams contain visual field maps as well as category-selective regions. Those category-specific regions process categories like faces, houses, words, or bodies (e.g. *object-selective*: Malach et al., 1995; *face-selective:* Kanwisher, McDermott, & Chun, 1997; *place-selective:* Aguirre, Zarahn, & D'Esposito, 1998; Epstein & Kanwisher, 1998; *word-selective:* Cohen et al., 2000; *body-selective:* Peelen & Downing, 2005.

In order to study the detailed neural computations of these category selective regions in visual cortex, one has to identify their cortical location first. The standard method is to perform a functional localizer scan, identifying the region of interest (ROI) that is selectively responding to the category of interest (e.g. by using a t-statistic). Consequently, the experiment of interest is performed, and the data are analyzed within the ROI previously identified. ROI approaches are advantageous for a variety of reasons, among which: (1) they allow hypothesis driven comparisons of signals within a specific area of interest across different conditions, (2) they increase statistical sensitivity in multi-subject analyses (Nieto-Castañón and Fedorenko, 2012) and (3) they reduce the number of multiple comparisons present in whole-brain analyses (Saxe et al., 2006). Additionally, ROIs frequently serve as seed regions for connectivity analyses and computational modeling (El Gazzar et al., 2019; Kautzky et al., 2018; Rondina et al., 2018; Vakli et al., 2018).

While the individual localizer approach has its benefits, it also comes with problems: first, a localizer scan is subject-specific and not necessarily representative of the population. Second, performing an accurate localizer scan before each experiment is costly in terms of scanning time, as well as in attention for the subject. The latter can result in fatigue during the actual experiment. Lastly, in some cases it is not possible to obtain a localizer, for example in patient populations as for example the congenitally blind (Bedny et al., 2011; Mahon et al., 2009; Striem-Amit et al., 2012a, 2012b, Van den Hurk et al., 2017) and individuals with visual agnosia/prosopagnosia (Barton, 2008; Gilaie-Dotan et al., 2009; Schiltz and Rossion, 2006; Sorger et al., 2007; Steeves

et al., 2006; Susilo et al., 2015). However, it may still be of interest to investigate functional or anatomical patterns within those populations, for example to compare them to typical individuals.

To overcome these problems, progressions in the field of cognitive neuroscience have led to the development of cortical atlases which allow localization of specific regions in a new, independent set of subjects by leveraging ROI-data from typical populations (e.g. Eickhoff et al. 2006, Frost and Goebel, 2012; Glasser et al., 2016; Rosenke et al., 2017; Wang et al., 2014). Next to providing independent data, this approach enables quantification of between-subject variability, as well as measures of prevalence and robustness of a region of interest. Recent atlases have mapped visual cortex retinotopically (Wang et al., 2014), cytoarchitectonically (Amunts et al., 2000; Caspers et al., 2013; Kujovic et al., 2013; Lorenz et al., 2015; Rosenke et al., 2017a; Rottschy et al., 2007) and using multimodal approaches (Glasser et al., 2016). To our knowledge, a gap in the field is a detailed atlas that delineates category-selective regions in lateral occipito-temporal and ventral temporal cortex.

In the present research, we aimed at (a) developing a functional atlas of category-selective visual cortex, (b) quantifying inter-subject variability of category-selective regions in visual cortex, and (c) validation of our atlas against existing atlases. We performed a localizer experiment in order to map category-selective regions, as well as a visual field mapping experiment to delineate early visual cortex in each participant. The experiment was performed using data of twenty healthy adults. The resulting atlas will be available in BrainVoyager (www.brainvoyager.com) and FreeSurfer (www.surfer.nmr.mgh.harvard.edu) file formats for surface analysis, as well as NifTI format for volumetric analysis (https://share.brainvoyager.com/index.php/s/m2E9oZTGWwXodRk).

## MATERIALS AND METHODS

### *Participants*

To obtain functional data, a total number of 20 participants (average age 30 ± 6.61) were recruited at Maastricht University. Two participants were left-handed, and the sample consisted of

10 women and 10 men. All participants were healthy with no history of neurological disease and had normal or corrected-to-normal vision. Written consent was obtained from each subject prior to scanning. All procedures were conducted with approval from the local Ethical Committee of the Faculty of Psychology and Neuroscience. After data acquisition, one participant's functional MRI scans were excluded from further analysis due to self-reported lack of attention on the stimuli and intermittent sleep.

*Data acquisition*

Participants underwent one scanning session of 1 hour at a 3T Siemens Prisma Fit (Erlangen, Germany). First, a whole brain, high resolution T1-weighted scan (MPRAGE) was acquired (repetition time/echo time = 2250/2.21 ms, flip angle = 9 ˚, field of view = 256 x 256 mm, number of slices = 192, 1 mm isovoxel resolution). Following that, six functional runs were acquired using a T2*-weighted sequence with the following parameters: repetition time/echo time = 2000/30 ms, flip angle = 77 ˚, field of view = 200 x 200 mm, number of slices = 35, slice thickness = 2 mm, in-plane resolution = 2 × 2 mm.

*Visual localizers*

<u>Category-selective regions in ventral temporal cortex</u>

In order to identify category-selective regions that respond preferentially to characters (pseudowords, numbers), bodies (whole bodies, limbs), places (houses, corridors) , faces (child, adult) and objects (cars, instruments), we used stimuli included in the fLoc functional localizer package (Stigliani et al., 2015). Eight stimuli of one of the five categories were presented in each miniblock design, each miniblock holding a duration of 4 seconds. To assure participant's attention, they were asked to perform an Oddball task, indicating with a button press when they saw a scrambled image instead of one of the categories. Each run consisted of 150 volumes.

hMT+

To localize the motion-selective area in middle temporal cortex (hMT+, Dumoulin et al., 2000; Zeki et al., 1991), we used stimuli as in Emmerling et al. (2016) and Zimmermann et al. (2011), which were based on Huk et al. (2002). During the first 5 volumes participants were presented with a fixation dot in the center of the screen. In the following, blocks moving and stationary dot patterns were alternated while the participants fixated on the fixation dot in the center of the screen. Moving dot blocks were 18 seconds long, while stationary blocks in-between had a duration of 10 seconds. The active screen filled with dots was circular. In total, each run consisted of 12 blocks of moving dots and 12 blocks of stationary dots. Furthermore, dots were presented either in the center of the screen, in the left visual hemifield, or in the right visual hemifield, while participants maintained fixation to the center of the screen. Stationary blocks were in the same three locations. The order of blocks was fixed (center moving, center static, left moving, left static, right moving, right static). For the moving dot blocks, dots moved outward and inward to the center of the circular field (left, center, right) in a steady speed until they reached the boundary of the circle, where they diminished. Each subject underwent two hMT+ localizer runs.

Early visual cortex

The visual retinotopic mapping run consisted of 304 volumes (TR = 2s). In the first 8 volumes a fixation dot was presented, followed by a high-contrast moving bar stimulus (1.33° wide) revealing a flickering checkerboard pattern (10 Hz). The checkerboard pattern varied in orientation and position for 288 volumes, concluding the run with 8 volumes of fixation dot presentation. The fixation was presented during the entire run and changed color at random time intervals. To keep participants' motivation and attention they were asked to count these color changes. The bar stimulus moved across the visual field in 12 discrete steps and remained at each position for 1 TR. The 12 different stimulus positions were randomized within each bar orientation. Each combination of orientation (4) and direction (2) represented one cycle. These eight different cycles were repeated three times in random order throughout the run (Senden et al., 2014). The width and height of the visual presentation subtended 15.5 x 15.5 degrees of visual angle.

*Preprocessing*

If not stated otherwise, data were preprocessed and analyzed using BrainVoyager 20.6 (Brain Innovation, Maastricht, The Netherlands). Anatomical data were inhomogeneity corrected and transformed to Talairach space (TAL, Talairach and Tournoux, 1988) by identifying the anterior commissure (AC) and posterior commissure (PC) and fitting the data to TAL space. Functional data were slice scan time corrected, motion corrected with intra-run alignment to the first functional run to account for movement between runs, and high-pass filtered (3 cycles). Next, the preprocessed functional data were coregistered to the inhomogeneity corrected anatomical image. Using the anatomical transformation files, all functional runs were normalized to TAL space. Based on the normalized anatomical data, we segmented the grey-white matter boundary for each brain and created a cortical surface. Next, the volumetric functional data were sampled on the cortical surface incorporating data from -1 to +3 mm along the vertex normals. Ultimately, we computed two general linear models (GLM), one for the three localizer runs for category-selective regions in ventral temporal cortex, and one for the hMT+ localization.

*Regions of interest*

All ROIs where manually defined in individual subject space on the cortical surface construction in BrainVoyager. For volumetric alignment and atlas generation, surface regions were transformed to volumetric regions by expanding them (-1 to +2 mm) along the vertex normals of the white-gray matter boundary.

<u>Retinotopic areas in occipital cortex</u>

Visual field maps were determined for each subject based on an isotropic Gaussian population receptive Field (pRF) model (Dumoulin and Wandell, 2008; Senden et al., 2014). The obtained pRF maps estimating the location and size of a voxel pRF were used to calculate

eccentricity and polar angle maps. The polar angle maps were projected onto inflated cortical surface reconstructions and used to define six topographic regions in occipital cortex (V1d, V2d, V3d and V1v, V2v, V3v, where d = dorsal and v = ventral) by identifying the reversals in polar angle representation at the lower vertical meridian (LVM), upper vertical meridian (UVM) or horizontal meridian (HM; DeYoe et al., 1996; Engel et al., 1997; Sereno et al., 1995).

Ventral and lateral category-selective areas

Each category (e.g. faces) was contrasted against the mean of all other categories to identify vertices that displayed a preference for the given category. Then we followed a two-step approach to define ROIs: First, for all categories we selected a statistical threshold of t = 3 for a whole brain map. Based on the thresholded activation map we identified ROIs in anatomically plausible locations (see details for each region below). Furthermore, in the case of an activation cluster transitioning into an adjacent one of the same visual category, we divided those clusters into separate ROIs by following the spatial gradient of t-values and separating the two areas at the lowest t-value. Based on insufficient activation pattern found for the 'objects' category, we dismissed that category from further analysis.

Face-selective regions (faces>all others) were identified in the mid lateral fusiform gyrus (mFus) and posterior lateral fusiform gyrus (pFus), which correspond to the fusiform face area (Kanwisher et al. 1997), as well as on the inferior occipital gyrus (IOG). Body-selective regions (bodies>all others) were observed in ventral temporal cortex on the occipital temporal sulcus (OTS), also known as fusiform body area (FBA, Peelen et al., 2009; Schwarzlose, 2005) and in lateral occipital cortex. There, we identified three different regions (Weiner and Grill-Spector, 2011) together forming the extrastriate body area (Downing et al., 2001), one anterior of hMT+ on the middle temporal gyrus (MTG), one posterior of hMT+ on the lateral occipital sulcus (LOS), and one ventral to hMT+, on the inferior temporal gyrus (ITG). Place-selective regions (places> all others) were observed in ventral temporal cortex on the collateral sulcus (CoS), corresponding to the parahippocampal place area (PPA, Epstein and Kanwisher, 1998), and on the transverse occipital sulcus (TOS, Hasson et al., 2003). Character-selective regions (characters > all others)

were identified in the posterior occipital temporal sulcus (pOTS) and a left-lateralized region in the mid occipital temporal sulcus (mOTS). Furthermore, we identified one character-selective regions in the inferior occipital sulcus (IOS). In the following, we will refer to each ROI by its anatomical nomenclature, as described in Stigliani et al. (2015). For reference, Table 1 provides an overview about each ROI's anatomical as well as functional name.

| anatomical | functional |
|---|---|
| mFus - faces | FFA-2 |
| pFus - faces | FFA-1 |
| IOG - faces | – |
| OTS - bodies | FBA |
| ITG - bodies | EBA |
| MTG - bodies | EBA |
| LOS - bodies | EBA |
| pOTS -characters | VWFA-1 |
| IOS - characters | - |
| TOS - places | - |
| CoS - places | PPA |
| hMT - motion | hMT |

**Table 1. Nomenclature for functional regions-of-interest (fROIs).** Each category-selective functional activation cluster can be described by functional category or anatomical location. In this article we describe category-selective ROIs using the anatomical nomenclature and provide this table as a reference. Functional abbreviations are as followed: *FFA*: fusiform-face area, *FBA*: fusiform-body area, *EBA*: extrastriate body area, *VWFA*: visual word form area, *PPA*: parahippocampal place area, *hMT*: human middle-temporal (cortex).

<u>hMT+</u>

Motion selective regions were identified by contrasting left, right and central visual field motion conditions vs. the equivalent stationary conditions and using a thresholded statistical map

with a minimum t-value of 3. Two subjects only showed functional activation for the contrasts at a t value of 2.5 in one hemisphere, which we allowed for these subjects. hMT+ was consistently located in the posterior inferio-temporal sulcus (pITS).

*Visual functional atlas (visfAtlas) generation*

After ROIs were defined for each subject in each subject's space, we utilized two normalization techniques to bring the data into a common space: (1) nonlinear-volumetric alignment (NVA) for volume and (2) cortex-based alignment (CBA) for surface space. Furthermore, as it is common that not every ROI can be identified in each of the subjects, we decided that an ROI had to be present in more than 50% of the subjects (N > 10) to be considered for a group atlas. The ROIs which were ultimately used for the group atlases and in how many subjects they were defined can be found in Table 2.

| ROI | N (LH) | N (RH) |
|---|---|---|
| mFus - faces | 13 | 15 |
| pFus - faces | 17 | 15 |
| IOG - faces | 14 | 15 |
| OTS - bodies | 14 | 13 |
| ITG - bodies | 17 | 17 |
| MTG - bodies | 16 | 15 |
| LOS - bodies | 15 | 16 |
| pOTS -characters | 16 | - |
| IOS - characters | 11 | - |
| TOS - places | - | 12 |
| CoS - places | 18 | 18 |
| hMT - motion | 18 | 16 |
| V1d | 19 | 19 |
| V2d | 19 | 19 |
| V3d | 14 | 16 |
| V1v | 19 | 19 |
| V2v | 19 | 19 |
| V3v | 17 | 19 |

**Table 2. Number of subjects per functional ROI (fROI).** Individual variability across people, keeping a strict statistical threshold, and stimulus choices results in not every fROI being identified in all participants. We chose to exclude ROIs from atlas generation that were defined in less than half the participants (N = 10). Abbreviations: *LH*: left hemisphere, *RH*: right hemisphere.

## Nonlinear-volumetric alignment (NVA)

First, surface regions that were defined on each subject's cortical surface were mapped to volumetric regions by expanding them (-1 to +2 mm) along each vertex normal of the white-gray matter boundary. Second, the volumetric regions were transformed back to native ACPC space. Next, the individual brains were registered to the MNI152 group average brain using the Advanced Normalization Tools (ANTS; https://sourceforge.net/projects/advants/). Finally, the resulting nonlinear transformation matrices were used to warp the functionally-defined regions of interest (fROIs) into the same orientation and reference frame. The specific code for the affine volume registration and nonlinear transformation can be found here: https://share.brainvoyager.com/index.php/s/m2E9oZTGWwXodRk. The resulting NVA-aligned regions were further processed in NifTi format using MATLAB (www.mathworks.com), see details below.

## Cortex-based alignment (CBA)

To generate a surface group average brain of the subjects, we used cortex-based alignment (CBA) to generate a dynamic average (subsequently called BVaverage, publicly available at https://share.brainvoyager.com/index.php/s/m2E9oZTGWwXodRk). CBA was performed for both hemispheres separately after inflation to a sphere with overlaid curvature information at various levels of resolution (Frost and Goebel, 2012; Goebel et al., 2006). First, during a rigid alignment, the spheres of each subject's hemisphere was rotated along three dimensions to best match the curvature pattern of a randomly chosen target hemisphere. The lower the variability between the two folding curvature patterns, the better the fit after rigid sphere rotation. Following the rigid alignment for all subjects, a non-rigid CBA was performed. Curvature patterns of each

subject were used in four different levels of anatomical detail. Starting from low anatomical detail, each subject's hemisphere was aligned to a group average out of all subjects. During this process, the group average was dynamically updated to most accurately average all hemispheres. This sequence was repeated for all levels of curvature detail, until the group average was updated based on the highest level of anatomical detail per subject. During the alignment, we (1) derived a group average for each hemisphere (BVaverage), as well as (2) a transformation indicating for each vertex on a single-subject cortical surface where it maps to on the group average. These transformation files were then used to map each individual subject's fROIs to the BVaverage.

Probabilistic maps for occipitotemporal cortex in volume and surface space

We generated probabilistic maps of all regions after NVA as well as CBA and each of the following was done in both group spaces: after individual subject fROIs were projected to the MNI152 and BVaverage, respectively, each group fROI was defined. For each voxel/vertex of a group fROIs, the number of subjects which shared that voxel/vertex of the fROI was divided by the total number of subjects ($voxel\ probability = \frac{number\ of\ subjects\ sharing\ voxel/vertex}{total\ number\ of\ subjects\ in\ fROI}$). Thus, a value of 0 at a vertex in the group fROI indicates a vertex did not belong to that fROI in any subject, a value of .5 means that it belonged to the fROI in half the subjects, a value of 1 indicates that it belonged to that functional region in the entire study population (Fig. 1).

Cross-validated predictability estimation and atlas generation

One interesting feature of those fROIs is the possibility to serve as a prior to estimate the localization of corresponding ROIs in a new subject's brain, eliminating the need for a dedicated localizer run in the new subject. To allow for a reasonable estimate on the confidence to find this region in a new subject, we performed an exhaustive cross-validation analysis of the volumetric (NVA) as well as surface (CBA) alignment. For each fold, we generated a group probabilistc fROI (G) and a left-out subject's individual fROI (I). We estimated the predictability of the group

probabilistic fROI by calculating the dice coefficient (DSC), a measure of similarity of two samples:

$$dsc = \frac{2|I \cap G|}{|I| + |G|}$$

A dice coefficient of zero indicates no predictability and a dice coefficient of 1 indicates perfect predictability. As we did in previous work (Rosenke et al., 2017a), we applied different threshold levels to the group probabilistic fROI (G) to predict the location of the left-out-subject (Fig.2). That means we created a liberal group probabilistic fROI including each vertex that was present in at least 1 subject. Then we sequentially increased the threshold up to the most conservative threshold where all subjects had to share a voxel/vertex for it to be included in the group map. For statistical assessment, we compared dice coefficients across the two alignment methods using a repeated measures analysis of variance (ANOVA) with individual regions as different entries, alignment method (CBA vs NVA) as within-subject factor and hemisphere as between-subject factor. We ran this comparison on two different thresholds: once on unthresholded group maps, and once on a threshold that produced - across regions and methods - the highest predictability, 0.2. Additionally, we ran paired permutation tests within each region on dice coefficient results at threshold 0.2. Finally, we calculated the mean ROI size for each hemisphere and ROI in square millimeter ($mm^2$, Fig. 3) and used a paired t-statistic to assess whether there was a systematic hemispheric difference in size across ROIs.

<u>Generating a visual functional atlas (visfAtlas) by assigning each voxel and vertex to a unique fROI</u>

The processes described below provide a non-overlapping tiling of the functionally defined regions in occipito-temporal cortex in surface as well as volume space (Fig. 4).

*Cortex based alignment:* The probability maps determine the probability that each vertex belongs to a given fROI. However, it is possible that a point on the brain may belong to more than one

probabilistic fROI. This overlap is more likely to occur along boundaries of neighboring functional regions. In order to assign a unique functional label to each vertex in the atlas, we generated a maximum-probability map (MPM) of each area, once in volume space (NVA) and once in surface space (CBA). Using the probabilistic fROIs, we determined which vertices were shared by more than one probabilistic fROI and assigned these vertices to a single fROI based on the area which showed the highest probability at that vertex (Eickhoff et al., 2005). In cases where two areas held the same probability value for one vertex, we averaged the probabilistic values of neighbors of that vertex for each of the fROIs. The degree of neighbors averaged was increased until the vertex had a higher probability value in one of the areas. Lastly, after all vertices were assigned in each of the MPM areas, we searched for individual vertices that were not connected to other vertices of the same ROI. We used a decision threshold where a minimum of at least one 3$^{rd}$ degree neighbor for each vertex had to be in the same group ROI for that vertex to be part of the group ROI. In cases where single vertices where detected, they were assigned to the ROI with the second-highest probabilistic value and same-ROI vertices in the immediate neighborhood.

*Nonlinear volume alignment:* The creation of a maximum probability map in volume space was identical to that for CBA as described above, except for the neighborhood search. The neighborhood search was not implemented in the same way as the 3D nature of the volume atlas would lead to inevitable differences in the MPM creation when compared to the surface atlas. Instead, neighborhood search was only performed for 3 immediately adjacent voxel (3$^{rd}$ degree neighbor) in all three dimensions.

*A visual functional atlas available in volume and surface space*

The unique tiling of functionally defined visua regions provides a functional atlas (visfAtlas) which we make available (1) in volume space, and (2) in surface space. In addition, we make this atlas available in multiple file formats. *Volume:* we publish the volumetric visfAtlas in MNI space in BrainVoyager file format (VOI file) and NifTi format, which can be read by a variety of software packages. *Surface:* we publish the visfAtlas in file formats compatible with Brain Voyager as well as FreeSurfer. Note, however, that the surface atlases are generated slightly

differently for each software. For BrainVoyager, we generated a publicly available dynamic group average brain (BVaverage) that will be available with the distributed atlas, details are described above. Since FreeSurfer (https://surfer.nmr.mgh.harvard.edu/) is commonly used with the fsaverage brain, an average surface of 39 individuals, we converted the individually defined fROIs from each subject to cortical surface space in FreeSurfer after running each subject through the recon-all pipeline. Then, we used the FreeSurfer CBA algorithm to bring each subject's fROIs to the fsaverage space. Further processing was done as described above and the same for both softwares. All files can be downloaded here: https://share.brainvoyager.com/index.php/s/m2E9oZTGWwXodRk.

*Functional selectivity of atlas fROIs*

When using a probabilistic atlas, it is of great interest not only to know how likely one would find a new subject's fROI in the same location, but also what signals would be picked up for that subject within an atlas-fROI. For example, are voxel/vertices in face-selective atlas fROIs selective for faces? To test the generalizability of our atlas, we performed a leave-subject-out selectivity analysis in volume space. Although alignment in surface space leads to an overall better between-subject alignment than normalized volume space does, we decided to run the cross-validation in suboptimal volume space, thereby assessing the results in a conservative way. The analysis calculates the percentage of voxel selective for each condition within a given fROI, where the fROI is defined on all subject's data except the one dataset used for the selectivity computation. This was repeated for all possible leave-subject-out combinations. First, for each subject individually we created a volume maximum probability map (MPM) based on the other N-1 subjects (leaving the target subject out). Then, for each individual voxel within each fROI in this MPM, we estimated the average response amplitude to each category across trials using the optimized Least Squares – Separate (LS-S) trial estimation approach as described by Mumford et al. (2012). Then, we created a 'winner map' for each fROI per subject, in which the condition index that yielded the strongest response was assigned to each voxel within the fROI. Per condition, we counted the number of winning voxels within the ROI, which we expressed as a

percentage of the total number of voxels in the fROI. This procedure was repeated for each subject (Fig. 5).

*Comparison of our visfAtlas to existing publicly available atlases and relevant fROIs*

How does the visfAtlas compare to published atlases available? While there is no complete occipitotemporal atlas yet, retinotopic areas have been published by Wang et al. (2014), a probabilistic CoS-places by Weiner et al. (2018) and a motion selective area hMT+ by Huang et al. (2019). We compared our visfAtlas to the existing surface maps by assessing their correspondence in Freesurfer's fsaverage space. For each fROI, we superimposed our MPM-ROIs onto the existing atlas-ROI (Fig 6). We quantified their correspondence by calculating the dice coefficient (see details in previous section) between our visfAtlas MPM-ROI and the respective other atlas. However, as the hMT+atlas by Huang et al. (2019) was not constrained by other regions, we calculated the dice coefficient between the extent of our probabilistic map and their fROI. Specifically, our hMT+ atlas-ROI is constrained by surrounding body-selective regions that compete for voxel selectivity. For the atlas generation in Huang et al. (2019), however, no functional activations other than motion-selectivity were used when defining the altas-hMT, making a comparison of both atlases an unequal comparison.

## RESULTS

*Superior spatial overlap after cortex-based alignment for retinitopic and category selective regions*

Using data from 19 healthy participants we aimed at generating a probabilistic atlas of occipito-temporal and ventral temporal cortex. Individually defined regions were normalized to group space using either (1) cortex based alignment (CBA) or (2) nonlinear volumetric alignment (NVA). Figure 1 displays three example regions, one early visual retinotopic region in occipital cortex (v1d), as well as two higher-order category-selective regions in ventral temporal cortex

(Cos-bodies and mFus-faces). Qualitatively, this resulted in a higher degree of consistency across subjects when group maps were normalized using CBA as compared to NVA. Both v1d and Cos-places display a high consistency in the group map center as indicated by yellow colored vertices, while centers are more variable after NVA alignment, most evident in v1d. For mFus-faces, both group maps display a greater degree of variability across subjects than the other two regions, potentially due to region size and/or greater anatomical variability.

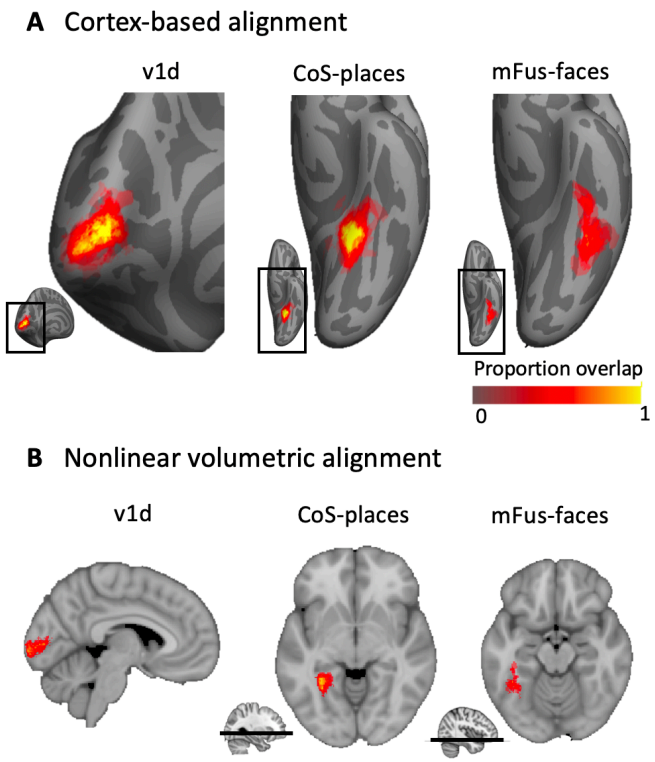


**Figure 1. Example probabilistic group maps in the left hemisphere after two brain alignments. (A)** Three example regions-of-interest (ROIs) are displayed where the most left column, v1d, shows an early visual cortex map and the middle and right columns display two higher-order visual category-selective regions in ventral temporal cortex, Cos-places and mFus-faces. Probability values range from 0 to 1 where 0 indicates no subject at a given vertex and 1 that all subjects in the probabilistic maps shared the given vertex. mFus-faces reveals less consistency as shown by a lower percentage of yellow-colored vertices. Bottom inset displays zoomed in location of the main figure. ***(B)*** Same ROIs as in A but after nonlinear volumetric alignment (NVA). Bottom inset for CoS-places and mFus-faces indicates the location of the axial slice in the volume.

To quantify which group alignment resulted in higher consistency and therewith predictability, we used the dice coefficent (DSC) and a leave-one-out cross-validation procedure to determine the predictability of finding the same region in a new subject. Moreover, we calculated the dice coefficient using different thresholds for the probabilistic group map, ranging from a liberal unthreshold (one subject at a given voxel/vertex is enough to assign it to the group map) maps to a conservative threshold where all N-1 subjects had to share a voxel/vertex to be assigned to the group map (Fig. 2).

For retinotopically defined regions, DSC's varied between 0.35 and 0.55 for peak probability after CBA, and between 0.30 and 0.40 after NVA. Especially regions with a lower predictability overall tended to show superior predictability after NVA for more conservative group thresholds (e.g. Fig. 2b, mFus-faces, TOS-bodies). For CBA, peak predictibility (DSC) for each region ranged from 0.1 to 0.55, while it ranged from 0.1 to 0.42 for NVA, with character-selective regions showing the lowest consistency for both alignments, closely followed by mFus- and IOG-faces. As the smaller regions seemed to show a greater variability we correlated ROI size (Fig. 3) with DSCs at a threshold of 0.2.

Quantitatively, CBA displayed an overall greater predictability across regions and thresholds (except for v3d), which was confirmed by a significant difference in alignment for both unthresholded ($F(1,34) = 20.12$, $p < .001$) and thresholded (0.2) probability maps, matching the highest DSC across regions and alignments($F(1,34) = 174.84$, $p < .001$). Additionally, there was no significant main effect for hemisphere (unthresholded: $p = .90$; thresholded: $p = .56$) and no interaction between alignment and hemisphere (unthresholded: $F(1,34) = .85$, $p = .36$, thresholded: $F(1,34) = 0.35$, $p = .56$). We followed up with a paired permutation test (across alignments) for the unthresholded DSC within each fROI. As there was no main effect for hemisphere (see above) and no significant difference in region size across hemispheres ($t(17) = -0.48$, $p = .64$, Fig. 3), permutation tests were performed on dice coefficients using an unthresholded group map prediction and averaged across hemispheres. Results show that CBA alignment has a higher predictability than NVA for all regions ($p < .05$), except for unthresholded: pOTS-characters (p =

1 1), IOS-characters (p = .81), v3d (p = .05), IOG-faces (p = .05) and thresholded: v3d (p = .05),
2 mFus (p = .70), IOG (p = .55), pOTS (p = 1), IOS (p = 1), OTS (p = .14).

3

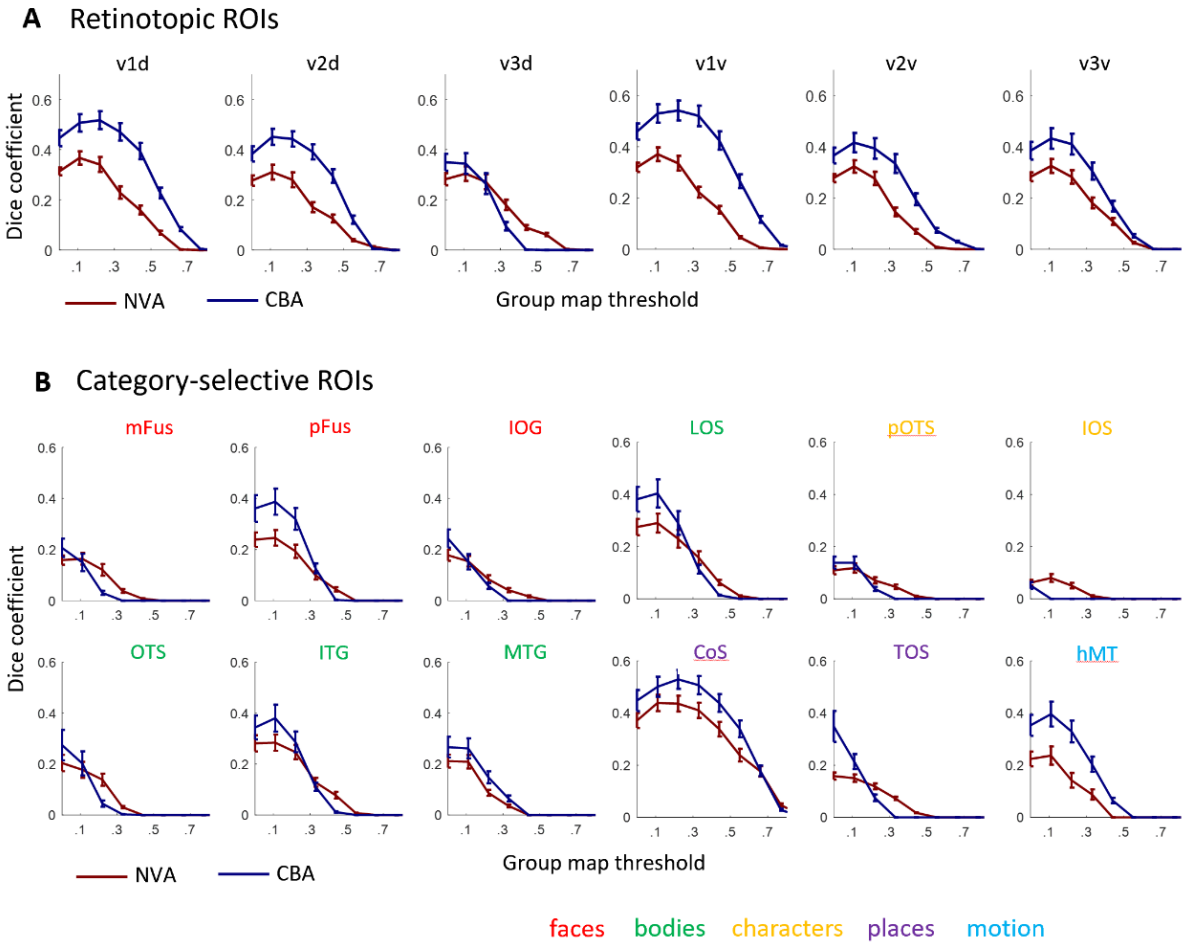


4

5 **Figure 2. Leave-one-out cross-validation predictability analysis using the dice coefficient (DSC) for retinotopic**
6 **regions (A) and category-selective regions (B).** *x-axis:* threshold of the probability map generated using N-1
7 subjects, y-axis: DSC. A DSC value of 1 indicates perfect overlap between the N-1 group map and the left out subject
8 0 indicates no overlap. *Blue lines*: DSC after CBA, *red lines*: DSC after NVA. Results for left and right hemisphere
9 were averaged per alignment method. *Red*: face-selective ROIs, *green*: body-selective ROIs, *yellow:* character-
10 selective ROIs, *light blue:* motion-selective ROI, *error bars*: standard error (SE) across the N-fold cross-validation.

11

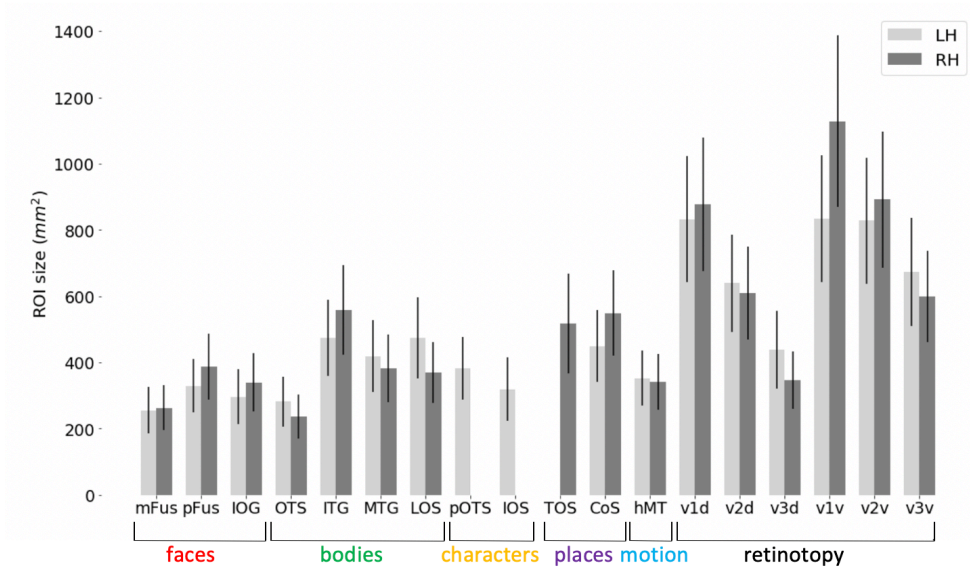


**Figure 3**. **fROI size across occipito-temporal cortex**. Average ROI size in surface space separately for the left hemisphere (LH, *light gray*) and right hemisphere (RH, *dark gray*). *Error bars*: standard error across subjects. Regions of X-axis are organized by category.

*A functional atlas of occipito-temporal cortex in volume and surface space*

By systematically varying the group map threshold for predicting a left-out subject's fROI, we established that a group map threshold of 0.2 allows for greatest predictability across regions. Using the 0.2 threshold, we generated a functional atlas of occipito-temporal cortex by generating a maximum probability map (MPM, see Methods for details). Figure 4 displays the resulting unique tiling of category-selective regions in stereotaxic space for surface (Fig. 4A) and volume (Fig. 4B) space. The visfAtlas is publically available in both surface as well as volume space to allow usage in a variety of analyses and in file formats for BrainVoyager and FreeSurfer for surface space as well as in volume space using the NifTi format (https://share.brainvoyager.com/index.php/s/m2E9oZTGWwXodRk).

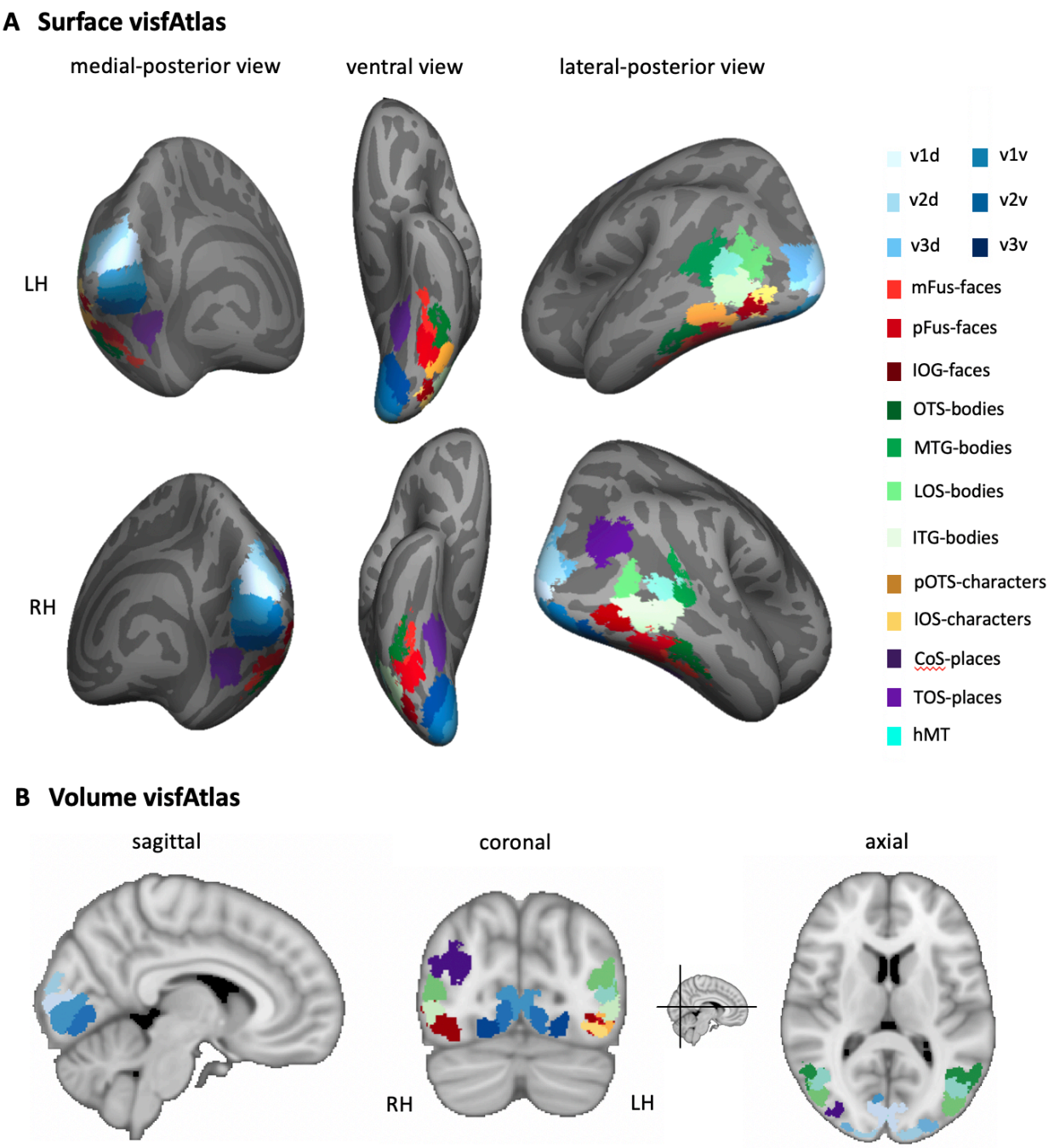


**Figure 4. Maximum-probability map (MPM) of occipito-temporal cortex functional regions-of-interest (fROIs).** (A) visfAtlas in surface space after cortex-based alignment. Each color displays a unique fROI group map thresholded at 0.2 of all subjects in which the given fROI could be identified. (B) Volume atlas using the same color coding as in surface space. Inset between coronal and axial view displays the slice location for coronal and axial slices, respectively. *LH*: left hemisphere, *RH*: right hemisphere.

*Generalizability of functional selectivity*

One of the advantages of a probabilistic atlas is the ability to locate a region of interest with a degree of certainty (as established using the dice coefficient analysis) in a new subject without the need to run a localizer itself. In order to quantify the atlas' generalizability, the selectivity of the category selective areas in new participants is a crucial metric. Therefore, we performed a leave-subject-out selectivity analysis in volume space to assess category-selectivity. For each fROI, we established the percentage of voxels that showed the strongest response to each available category (Fig. 5, see Methods for details of selectivity estimation). For all category selective regions, we confirmed that the category it is selective for indeed yields the highest percentage of voxels across subjects. Face-selective fROIs (Fig. 5, top left) contain 52-72% (lowest to highest fROI) face-selective voxel responses (*red*). The second-highest selectivity is body-selective (*green*) with 10-43% on average across subjects, followed by character-selective regions (*gray*) with 2-25%. Body-selective regions (Fig. 5, top right) contain the highest proportion of body-selective voxels for lateral bod-selective regions (80-94%), with lowest proportions for ventral OTS-bodies in left and right hemisphere (46-55%). The second-largest number of voxel-selectivity is face selectivity (1- 40%). Place-selective fROIs (Fig. 5, bottom left) show a large proportion of voxels with their preferred place selectivity (*purple*, 77-82%), followed by up to 21% body-selective voxel. Character-selective ROIs (Fig 5., bottom right) on the other hand contain 41 - 52% character-selective voxel, followed by up to 38% body-selective voxels.

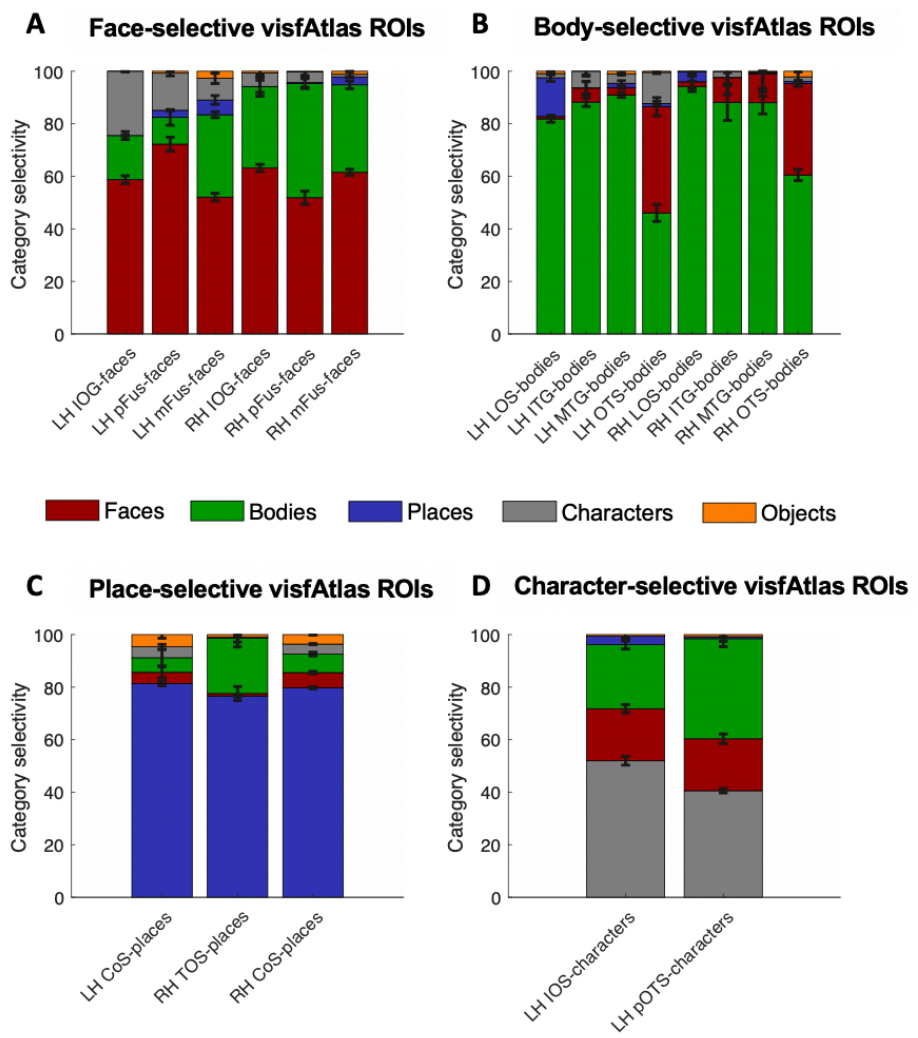


**Figure 5. Selectivity analysis for category-selective fROIs using a leave-subject-out cross-validation procedure.** For each major category - faces, bodies, places, characters – proportions of category selectivity are displayed with each region's preferred category as the bottom bar of each stacked bar graph. *Error bars*: Selectivity estimate across all left-out subjects.

*Similarities between previously published atlas areas and our visfAtlas*

In order to establish the correspondence of our probabilistic functional atlas to other atlases, we made quantitative comparisons to existing atlases of one or multiple regions localized with comparable stimuli. As retinotopic atlases are frequently used to define early visual cortices in new subjects, we wanted to compare our retinotopic areas v1-v3 dorsal and ventral to a group atlas

of retinotopic visual areas aligned to the *fsaverage brain* by Wang et al. (2014). To assess the correspondence between the two atlases we computed the dice coefficient (see Methods for details) between the existing group atlas and our visfAtlas region for each region separately. Qualitatively, v1d and v1v from both atlases show a high degree of overlap and correspondence decreases when moving to the dorsal and ventral v2 and v3 regions (Fig. 6A). In addition, there is a shift in the right hemisphere region location that is not present in the left hemisphere. This observation is confirmed with high dice coefficients for v1d and v1v in the left hemisphere (0.81 and 0.89, respectively) and lower dice coefficients in the right hemisphere (v1d: 0.70, v1v: 0.72). Both dorsally and ventrally, the difference between hemispheres becomes more prominent (LH: v2d: 0.61, v3d: 0.53, v2v: 0.89, v3v: 0.59; RH: v2d: 0.34, v3d: 0.05, v2v: 0.54, v3v: 0.31).

In a similar fashion to the retinotopic regions, we compared a category-selective region - the CoS-places fROI - to a published probabilistic version by Weiner et al. (2018) which used the same localizer for their study. Both atlases display a high correspondence, with a higher dice coefficient in the left hemisphere than in the right hemisphere (LH: 0.85, RH: 0.61). On lateral occipito-temporal cortex we compared a recently published motion selective group area of hMT+that has been defined using data from 509 adults. As their group fROI was not bound by body-selective regions with a maximum probability map (MPM) as ours, we chose to compare their group hMT+map with our probabilistic hMT+ that is also not restricted with body-selective areas. In the left hemisphere the dice coefficient is 0.59, and 0.69 in the right hemisphere and therewith showing a greater consistency in the right hemisphere.

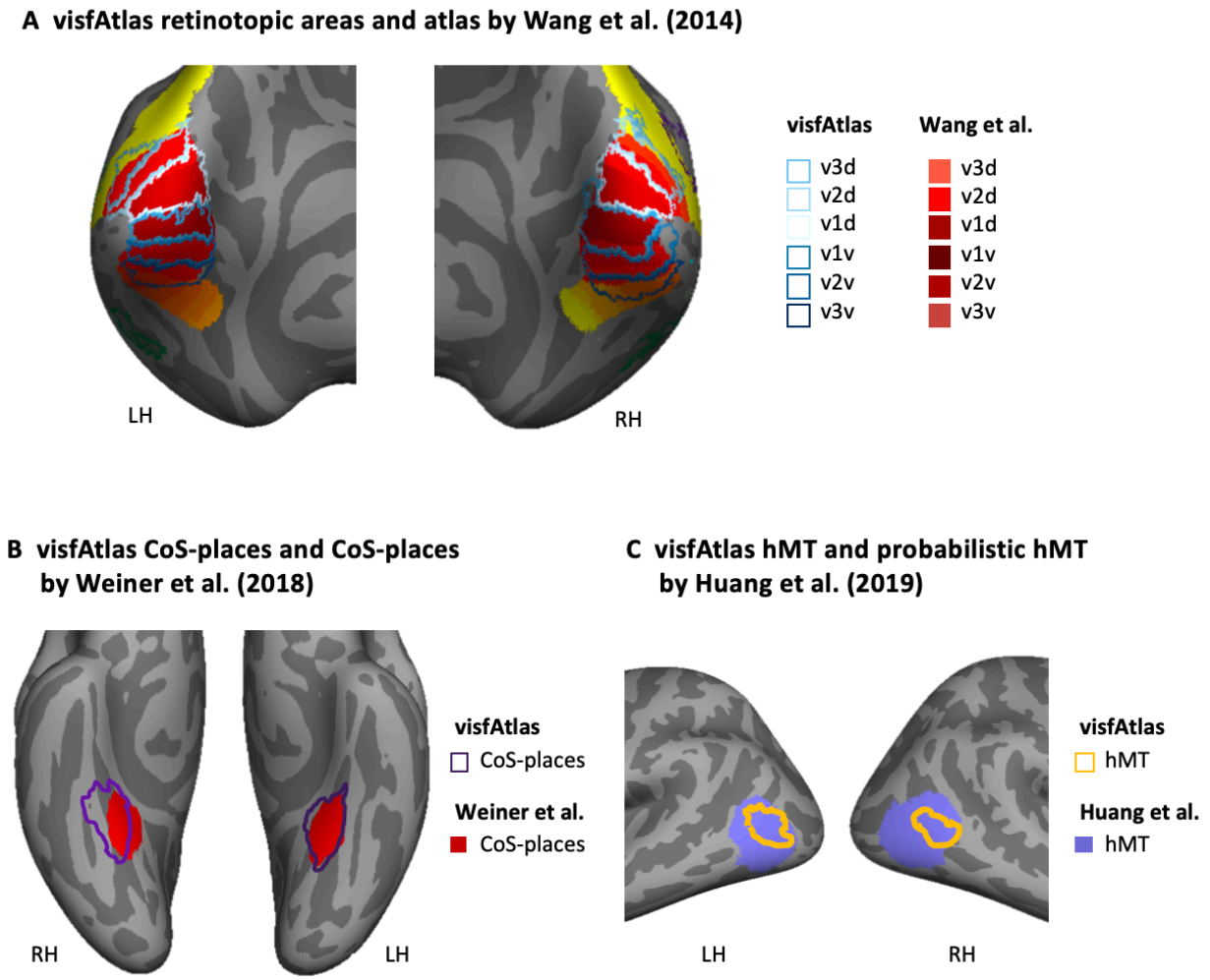


**Figure 6. Similarities across different probabilistic atlases and the visfAtlas.** Superposition of our visfAtlas onto three existing probabilistic atlases. (A) A comparison of V1-V3 dorsal and ventral of the retinotopic atlas published by Wang et al (2014) and our respective visfAtlas regions. Regions are presented on a medial-occipital view of the fsaverage group brain. (B) CoS-places as published by Weiner et al (2018) and visfAtlas CoS-places, localized using the same stimuli and visualized using a ventral view of the fsaverage brain. (C) A probabilistic ROI of motion-selective hMT+published by Huang et al. (2019) and our probabilistic ROI, noteworthy, not the MPM as it is not restricted by surrounding body-selective regions, of hMT+shown in a lateral view of the fsaverage brain. *Solid ROIs*: published atlases by other groups; *outlined ROIs*: our visfAtlas ROIs. LH: left hemisphere; RH: right hemisphere.

## DISCUSSION

We generated a cross-validated functional parcellation of occipito-temporal visual cortex, including early-visual cortex retinotopic regions as well as category-selective regions. Additionally, we estimated predictability and selectivity for left-out subjects. We show that cortex-based alignment (CBA) outperforms nonlinear-volumetric alignment (NVA) in most cases and that each probabilistic functional region maintains between 40% and 94% of its own category's response in a left-out subject (Fig. 5), suggesting a higher precision of our surface-based atlas while also demonstrating its utility in volumetric MNI space. To our knowledge this is the first extensive cross-validated probabilistic atlas of category-selective regions in ventral temporal cortex besides CoS-places published by Weiner et al. (2018). We make this functional atlas of occipito-temporal cortex available in surface as well as volume space, together with a new BrainVoyager surface average that can be used for any surface-analysis (https://share.brainvoyager.com/index.php/s/m2E9oZTGWwXodRk).

### *Superior consistency of functional group regions after cortex-based alignment: Implications*

Spatial consistency in both retinotopic as well as category-selective regions was higher after CBA as compared to NVA (Fig. 3). The superior performance of CBA is in agreement with previous findings of retinotopic regions (Wang et al., 2014) as well as cytoarchitectonic regions and their relationship to functional parcellations of the ventral visual stream (Rosenke et al., 2017a, 2017b). The greater consistency of functional parcellations highlights a strong coupling between macroanatomical landmarks and functional regions, which has indeed been observed in early visual cortex between V1 and the calcarine sulcus (Hinds et al., 2008), in intermediate visual areas between V3A as well as human V4 and the transverse occipital and collateral sulcus, respectively (Nasr et al., 2011; Tootell et al., 1997; Witthoft et al., 2014), as well as in lateral visual cortex for motion-selective hMT+ and two underlying sulci (Dumoulin et al., 2000; Weiner and Grill-Spector, 2011). Similarly, various category-selective regions in ventral temporal cortex have shown a macroanatomy-function coupling (Grill-Spector and Weiner, 2014; Weiner et al., 2018, 2014; Weiner and Grill-Spector, 2013).

Historically, functional regions were assumed to have a greater variability (a) in higher-visual cortices, as well as (b) a weak co-occurrence with macroanatomical landmarks. However, as pointed out using various anatomical-functional correspondences in the paragraph above and supported by higher functional consistency after microanatomical alignment in recent work (Wang et al., 2014), this does not hold true. In accordance with this, our leave-one-out cross-validation procedure shows that five regions sensitive to visual stimulation of specific categories (pFus-faces, LOS-bodies, ITG-bodies, CoS-places, motion-selective hMT+, Fig. 3) have a similar amount of overlap as retinotopic regions outside of V1. Other functional regions, however, show more variability (e.g. mFus-faces, pOTS-characters, MTG-bodies, Fig. 3, see also Frost and Goebel, 2012). This highlights how other factors besides location in the cortical hierarchy play a role in the consistency of functional regions, and we discuss a few possibilities here: First, it may be a factor of region size, as even though the dice coefficient takes overall region size into account, region size still correlates with dice coefficient results (Rosenke et al., 2017a). Future efforts should include the exploration and development of measures that are independent of region size. Second, functional variability can in part be influenced by the functional-macroanatomical consistency across subjects. For example, the anterior tip of a macroanatomical landmark, the mid-fusiform sulcus (MFS), has been shown to be a more stable predictor of functional regions than its length or posterior section (Weiner et al., 2014). This indicates that not all anatomical structures that get aligned during CBA have to have an equally strong relationship to a functional region of interest. Third, the quality of the macroanatomical alignment across subjects may vary across cortical locations due to greater anatomical variability across individuals. While results of cortex-based alignment are often seen as precise and superior to other methods, it is easily overlooked that functional consistency is often evaluated under the assumption that anatomical alignment is perfect. However, Frost and Goebel (2012, 2013) showed that while CBA outperforms non-aligned and volumetrically-aligned anatomical landmarks, macroanatomical landmarks still show a degree of variability unique to each landmark. One can imagine that for smaller landmarks with greater variability, e.g. the partially fragmented occipito-temporal sulcus (OTS), CBA will be less able to align landmarks compared to highly consistent anatomical structures. A future, more advanced, alignment scheme could take such emerging knowledge into account by using non-homogeneous regional weights for curvature landmarks.

*Structures defined in maximum probability map are category specific*

As the main purpose of a functional atlas is to allow generalization to new individuals, confirmation and validation of the functional selectivity of the delineated areas is crucial. We used a leave-one-out approach to quantify the generalizability of our maximum probability map, and demonstrate that voxels within a region-of-interest are highly selective to the category that the ROI is known to respond to. This is an important confirmation of one of the underlying assumptions of functional atlases: a (macro-)anatomical correspondence to function (Grill-Spector and Weiner, 2014; Weiner et al., 2018, 2014; Weiner and Grill-Spector, 2013), which can be utilized when aligning a new subject's macroanatomy to the macroanatomy an existing functional atlas is based on.

As can be observed in Figure 5, for each category-selective region, the largest proportion of voxel selectivity is that of the own category with the lowest overall proportion for word-selective regions (Fig. 5, bottom right). Furthermore, the highest proportion of own-category-selectivity can be found in lateral body-selective regions (Fig. 5, top right). One possible explanation for the variability in this location is the proximity to other category selective regions. For example, when comparing face-and body selective areas in ventral temporal cortex (see Fig. 4 A for details), they are very close together as well as adjacent, when compared to body-selective regions in lateral occipital cortex. This close proximity increases the likelihood of overlapping functional specificity of atlas boundaries that may or may not align precisely with a new subject's functional selectively. Next, areas in ventral temporal cortex tend to be smaller. Due to the nature of our selectivity measure, dividing the number of category-preferring voxel within a region by the total number is more drastically influenced by single voxels in smaller regions as compared to larger regions.

*Consistent functional loci across different atlases*

Comparing our visfAtlas regions to existing atlases can highlight the effects of (1) different localizer stimuli (e.g. Fig 6 A & C), as well as (2) effects of the number of subjects included in a group map (Fig. 6). With retinotopy being one of the fundamental organizational principles of visual cortex (Arcaro et al., 2009; Brewer et al., 2005; Dumoulin and Wandell, 2008; Orban et al., 2004; Sereno et al., 1995) we aimed at comparing our retinotopic regions V1-V3 dorsal and ventral to an existing atlas published by Wang et al. (2014). Interestingly, V1d and V1v show a high degree of overlap across both atlases (Fig. 6A), especially in the left hemisphere. Right hemisphere V1 of the visfAtlas extends more dorsally, consequently shifting other right hemisphere retinotopic regions as compared to the atlas by Wang et al. (2014). In addition, we compared our visfAtlas CoS-places to a CoS-places published by Weiner et al. (2018), who used the same localizer for their atlas as well as the same statistical threshold for defining CoS-places in each subject (t=3). Interestingly, also here the probabilistic ROIs differ more in the right than left hemisphere (Fig. 6B). However, we found no differences across hemispheres for region size as well as predictability, providing evidence against our assumptions. The fact that the right hemisphere showed more differences across atlases could be due to a variety of factors.

Next to retinotopic regions of early visual cortex, we also compared our motion-selective hMT+ to a recently published probabilistic atlas, based on a large-scale dataset of >500 participants (Huang et al., 2019). In this work, a visual localizer (moving concentric rings which expanded or contracted) different from ours (circular block of dots moving in several directions) was used and might explain the slightly different loci of the hMT+ probability map presented here. Our hMT+ localizer may include less medial superior temporal (MST) area due to the differences. However, the probabilistic maps are difficult to compare due to the large difference in sample size between their and our study. The region published by Huang et al. (2019) has a surface area more than double from ours, highlighting the inter-subject variability in hMT+ location.

Ultimately, besides the differences across atlas regions, each of the three atlases compared with our visfAtlas defines cortical areas with the same functional locus, highlighting the utility of functional atlases for future neuroimaging studies.

*Conclusion and future uses*

To this date, no probabilistic atlas has been published which contains such an extensive set of functional regions in occipito-temporal cortex. The present study shows that most of the category-selective regions can indeed be found in new subjects at predicted locations with functional magnetic resonance imaging. Additionally, these regions show high specificity towards their respective categories. Finally, we showed that these selectivity results are generalizable by means of a leave-one-out analysis. Future studies should aim at extending this atlas by including dynamic stimuli in addition to static, since those are more suitable for ventral temporal correct and further category-selective regions in lateral occipital cortex could be delineated using dynamic stimuli (Beauchamp et al., 2003; Grossman and Blake, 2002; Pitcher et al., 2011; Puce et al., 1996).

The functional atlas of occipito-temporal cortex in both, surface and volume space, is available in most commonly used imaging data formats (https://share.brainvoyager.com/index.php/s/m2E9oZTGWwXodRk). Our atlas may prove especially useful for (a) predicting a region of interest when no localizer data is available, saving scanning time and expenses or (b) for comparison's across modalities as patient populations as for example patients who are brain lesioned (Barton, 2008; de Heering and Rossion, 2015; Gilaie-Dotan et al., 2009; Schiltz and Rossion, 2006; Sorger et al., 2007; Steeves et al., 2006) or congenitally blind (Bedny et al., 2011; Mahon et al., 2009; Striem-Amit et al., 2012; van den Hurk et al., 2017).

**Acknowledgements**

We would like to thank Martin Frost for advice with the experimental design, Kevin S. Weiner for feedback on individual definitions of regions-of-interest and Kevin S. Weiner and Kalanit Grill-Spector for analysis suggestions. RG was supported by the European FET Flagship project 'Human Brain Project' FP7-ICT-2013-FET-F/604102 Grant Agreements, No. 7202070 (SGA1) and No. 785907 (SGA2).

## References


Amunts, K., Malikovic, A., Mohlberg, H., Schormann, T., Zilles, K., 2000. Brodmann's areas 17 and 18 brought into stereotaxic pace - where and how variable? . Neuroimage 11, 66–84.

Arcaro, M.J., McMains, S.A., Singer, B.D., Kastner, S., 2009. Retinotopic organization of human ventral visual cortex. J Neurosci 29, 10638–10652. https://doi.org/29/34/10638 [pii]\r10.1523/JNEUROSCI.2807-09.2009

Barton, J.J.S., 2008. Structure and function in acquired prosopagnosia: lessons from a series of 10 patients with brain damage. J. Neuropsychol. 2, 197. https://doi.org/10.1348/174866407X214172

Beauchamp, M.S., Lee, K.E., Haxby, J. V., Martin, A., 2003. fMRI Responses to Video and Point-Light Displays of Moving Humans and Manipulable Objects. J. Cogn. Neurosci. 15, 991–1001. https://doi.org/10.1162/089892903770007380

Bedny, M., Pascual-Leone, A., Dodell-Feder, D., Fedorenko, E., Saxe, R., 2011. Language processing in the occipital cortex of congenitally blind adults. Proc. Natl. Acad. Sci. U. S. A. 108, 4429–34. https://doi.org/10.1073/pnas.1014818108

Brewer, A.A., Liu, J., Wade, A.R., Wandell, B.A., 2005. Visual field maps and stimulus selectivity in human ventral occipital cortex 8, 1102–1109. https://doi.org/10.1038/nn1507

Caspers, J., Zilles, K., Eickhoff, S.B., Schleicher, A., Mohlberg, H., Amunts, K., 2013. Cytoarchitectonical analysis and probabilistic mapping of two extrastriate areas of the human posterior fusiform gyrus. Brain Struct Funct 218, 511–526. https://doi.org/10.1007/s00429-012-0411-8

de Heering, A., Rossion, B., 2015. Rapid categorization of natural face images in the infant right hemisphere. Elife 4, 1–14. https://doi.org/10.7554/elife.06564

DeYoe, E. a, Carman, G.J., Bandettini, P., Glickman, S., Wieser, J., Cox, R., Miller, D., Neitz, J., 1996. Mapping striate and extrastriate visual areas in human cerebral cortex. Proc. Natl. Acad. Sci. U. S. A. 93, 2382–2386. https://doi.org/10.1073/pnas.93.6.2382

Downing, P.E., Downing, P.E., Jiang, Y., Jiang, Y., Shuman, M., Shuman, M., Kanwisher, N., Kanwisher, N., 2001. A cortical area selective for visual processing of the human body. Science 293, 2470–3. https://doi.org/10.1126/science.1063414

Dumoulin, S.O., Bittar, R.G., Kabani, N.J., Baker, C.L., Le Goualher, G., Bruce Pike, G., Evans, a C., 2000. A new anatomical landmark for reliable identification of human area V5/MT: a quantitative analysis of sulcal patterning. Cereb. Cortex 10, 454–463. https://doi.org/10.1093/cercor/10.5.454

Dumoulin, S.O., Wandell, B.A., 2008. Population receptive field estimates in human visual cortex. Neuroimage 39, 647–660. https://doi.org/10.1016/j.neuroimage.2007.09.034

Eickhoff, S.B., Stephan, K.E., Mohlberg, H., Grefkes, C., Fink, G.R., Amunts, K., Zilles, K., 2005. A new SPM toolbox for combining probabilistic cytoarchitectonic maps and functional imaging data. Neuroimage 25, 1325–1335. https://doi.org/10.1016/j.neuroimage.2004.12.034

El Gazzar, A., Cerliani, L., Van Wingen, G., Thomas, R.M., 2019. Simple 1-D Convolutional Networks for Resting-State fMRI Based Classification in Autism, in: Proceedings of the International Joint Conference on Neural Networks. Institute of Electrical and Electronics Engineers Inc. https://doi.org/10.1109/IJCNN.2019.8852002

Emmerling, T.C., Zimmermann, J., Sorger, B., Frost, M.A., Goebel, R., 2016. Decoding the direction of imagined visual motion using 7 T ultra-high field fMRI. Neuroimage 125, 61–73. https://doi.org/10.1016/j.neuroimage.2015.10.022

Engel, S.A., Glover, G.H., Wandell, B.A., 1997. Retinotopic organization in human visual cortex and the spatial precision of functional MRI. Cereb Cortex 7, 181–192.

Epstein, R., Kanwisher, N., 1998. A cortical representation of the local visual environment. Nature 392, 598–601. https://doi.org/10.1038/33402

Frost, M.A., Goebel, R., 2013. Functionally informed cortex based alignment: an integrated approach for whole-cortex macro-anatomical and ROI-based functional alignment. Neuroimage 83, 1002–1010. https://doi.org/10.1016/j.neuroimage.2013.07.056

Frost, M.A., Goebel, R., 2012. Measuring structural-functional correspondence: spatial variability of specialised brain regions after macro-anatomical alignment. Neuroimage 59, 1369–1381. https://doi.org/10.1016/j.neuroimage.2011.08.035

Gilaie-Dotan, S., Perry, A., Bonneh, Y., Malach, R., Bentin, S., 2009. Seeing with profoundly deactivated mid-level visual areas: Non-hierarchical functioning in the human visual cortex.

Cereb. Cortex 19, 1687–1703. https://doi.org/10.1093/cercor/bhn205

Glasser, M.F., Coalson, T.S., Robinson, E.C., Hacker, C.D., Harwell, J., Yacoub, E., 2016. A multi-modal parcellation of human cerebral cortex. Nat. Publ. Gr. 536, 171–178. https://doi.org/10.1038/nature18933

Goebel, R., Esposito, F., Formisano, E., 2006. Analysis of functional image analysis contest (FIAC) data with brainvoyager QX: From single-subject to cortically aligned group general linear model analysis and self-organizing group independent component analysis. Hum Brain Mapp 27, 392–401. https://doi.org/10.1002/hbm.20249

Goodale, M.A., Milner, A.D., Jakobson, L.S., Carey, D.P., 1991. A neurological dissociation between perceiving objects and grasping them. Nature. https://doi.org/10.1038/349154a0

Grill-Spector, K., Weiner, K.S., 2014. The functional architecture of the ventral temporal cortex and its role in categorization. Nat. Rev. Neurosci. 15, 536–548. https://doi.org/10.1038/nrn3747

Grossman, E.D., Blake, R., 2002. Brain areas active during visual perception of biological motion. Neuron 35, 1167–1175. https://doi.org/10.1016/S0896-6273(02)00897-8

Hasson, U., Harel, M., Levy, I., Malach, R., 2003. Large-scale mirror-symmetry organization of human occipito-temporal object areas. Neuron 37, 1027–1041. https://doi.org/10.1016/S0896-6273(03)00144-2

Hinds, O.P., Rajendran, N., Polimeni, J.R., Augustinack, J.C., Wiggins, G., Wald, L.L., Diana Rosas, H., Potthast, A., Schwartz, E.L., Fischl, B., 2008. Accurate prediction of V1 location from cortical folds in a surface coordinate system. Neuroimage 39, 1585–1599. https://doi.org/10.1016/j.neuroimage.2007.10.033

Huang, T., Chen, X., Jiang, J., Zhen, Z., Liu, J., 2019. A probabilistic atlas of the human motion complex built from large-scale functional localizer data. Hum. Brain Mapp. 40, hbm.24610. https://doi.org/10.1002/hbm.24610

Huk, A.C., Dougherty, R.F., Heeger, D.J., 2002. Retinotopy and functional subdivision of human areas MT and MST. J. Neurosci. 22, 7195–205. https://doi.org/20026661

Kanwisher, N.G., McDermott, J., Chun, M.M., 1997. The Fusiform Face Area: A Module in Human Extrastriate Cortex Specialized for Face Perception. J. Neurosci. 17, 4302–4311.

Kautzky, A., Seiger, R., Hahn, A., Fischer, P., Krampla, W., Kasper, S., Kovacs, G.G., Lanzenberger, R., 2018. Prediction of Autopsy Verified Neuropathological Change of Alzheimer's Disease Using Machine Learning and MRI. Front. Aging Neurosci. 10. https://doi.org/10.3389/fnagi.2018.00406

Kujovic, M., Zilles, K., Malikovic, A., Schleicher, A., Mohlberg, H., Rottschy, C., Eickhoff, S.B., Amunts, K., 2013. Cytoarchitectonic mapping of the human dorsal extrastriate cortex. Brain Struct Funct 218, 157–172. https://doi.org/10.1007/s00429-012-0390-9

Lorenz, S., Weiner, K.S., Caspers, J., Mohlberg, H., Schleicher, A., Bludau, S., Eickhoff, S.B., Grill-Spector, K., Zilles, K., Amunts, K., 2015. Two New Cytoarchitectonic Areas on the Human Mid-Fusiform Gyrus. Cereb Cortex 1–13. https://doi.org/10.1093/cercor/bhv225

Mahon, B.Z., Anzellotti, S., Schwarzbach, J., Zampini, M., Caramazza, A., 2009. Category-Specific Organization in the Human Brain Does Not Require Visual Experience. Neuron 63, 397–405. https://doi.org/10.1016/j.neuron.2009.07.012

Mishkin, M., Ungerleider, L.G., Macko, K. a, 1983. Object vision and spatial vision: Two central pathways. Trends Neurosci. 6, 414–417. https://doi.org/Doi 10.1016/0166-2236(83)90190-X

Mumford, J.A., Turner, B.O., Ashby, F.G., Poldrack, R.A., 2012. Deconvolving BOLD activation in event-related designs for multivoxel pattern classification analyses. Neuroimage 59, 2636–2643. https://doi.org/10.1111/j.1751-9004.2009.00170.x.Experience

Nasr, S., Liu, N., Devaney, K.J., Yue, X., Rajimehr, R., Ungerleider, L.G., Tootell, R.B.H., 2011. Scene-selective cortical regions in human and nonhuman primates. J. Neurosci. 31, 13771–13785. https://doi.org/10.1523/JNEUROSCI.2792-11.2011

Nieto-Castañón, A., Fedorenko, E., 2012. Subject-specific functional localizers increase sensitivity and functional resolution of multi-subject analyses. Neuroimage 63, 1646–1669. https://doi.org/10.1016/j.neuroimage.2012.06.065

Orban, G.A., Van Essen, D., Vanduffel, W., 2004. Comparative mapping of higher visual areas in monkeys and humans. Trends Cogn. Sci. 8, 315–324. https://doi.org/10.1016/j.tics.2004.05.009

Peelen, M. V., Glaser, B., Vuilleumier, P., Eliez, S., 2009. Differential development of

selectivity for faces and bodies in the fusiform gyrus. Dev. Sci. 12, 16–25. https://doi.org/10.1111/j.1467-7687.2009.00916.x

Pitcher, D., Dilks, D.D., Saxe, R.R., Triantafyllou, C., Kanwisher, N., 2011. Differential selectivity for dynamic versus static information in face-selective cortical regions. Neuroimage 56, 2356–2363. https://doi.org/10.1016/j.neuroimage.2011.03.067

Puce, A., Allison, T., Asgari, M., Gore, J.C., McCarthy, G., 1996. Differential sensitivity of human visual cortex to faces, letterstrings, and textures: A functional magnetic resonance imaging study. J. Neurosci. 16, 5205–5215. https://doi.org/10.1523/jneurosci.16-16-05205.1996

Rondina, J.M., Ferreira, L.K., de Souza Duran, F.L., Kubo, R., Ono, C.R., Leite, C.C., Smid, J., Nitrini, R., Buchpiguel, C.A., Busatto, G.F., 2018. Selecting the most relevant brain regions to discriminate Alzheimer's disease patients from healthy controls using multiple kernel learning: A comparison across functional and structural imaging modalities and atlases. NeuroImage Clin. 17, 628–641. https://doi.org/10.1016/j.nicl.2017.10.026

Rosenke, M., Weiner, K.S., Barnett, M.A., Zilles, K., Amunts, K., Goebel, R., Grill-Spector, K., 2017a. A cross-validated cytoarchitectonic atlas of the human ventral visual stream. Neuroimage 1–14. https://doi.org/10.1016/j.neuroimage.2017.02.040

Rosenke, M., Weiner, K.S., Barnett, M.A., Zilles, K., Amunts, K., Goebel, R., Grill-Spector, K., 2017b. Data on a cytoarchitectonic brain atlas: effects of brain template and a comparison to a multimodal atlas. Data Br. 12, 327–332. https://doi.org/10.1016/j.dib.2017.04.007

Rottschy, C., Eickhoff, S.B., Schleicher, A., Mohlberg, H., Kujovic, M., Zilles, K., Amunts, K., 2007. Ventral visual cortex in humans: Cytoarchitectonic mapping of two extrastriate areas. Hum. Brain Mapp. 28, 1045–1059.

Saxe, R., Brett, M., Kanwisher, N., 2006. Divide and conquer: a defense of functional localizers. Neuroimage 30, 1088–1089. https://doi.org/10.1016/j.neuroimage.2005.12.062

Schiltz, C., Rossion, B., 2006. Faces are represented holistically in the human occipito-temporal cortex. Neuroimage 32, 1385–1394. https://doi.org/10.1016/j.neuroimage.2006.05.037

Schwarzlose, R.F., Baker, C.I., Kanwisher, N., 2005. Separate Face and Body Selectivity on the Fusiform Gyrus. J. Neurosci. 25, 11055–11059. https://doi.org/10.1523/JNEUROSCI.2621-

05.2005

Senden, M., Reithler, J., Gijsen, S., Goebel, R., 2014. Evaluating Population Receptive Field Estimation Frameworks in Terms of Robustness and Reproducibility. PLoS One 9, e114054. https://doi.org/10.1371/journal.pone.0114054

Sereno, M.I., Dale, a M., Reppas, J.B., Kwong, K.K., Belliveau, J.W., Brady, T.J., Rosen, B.R., Tootell, R.B.H., Series, N., May, N., 1995. Borders of Multiple Visual Areas in Humans Revealed by Functional Magnetic Resonance Imaging Borders of Multiple Visual Areas in Humans Revealed by Functional Magnetic Resonance Imaging 268, 889–893.

Sorger, B., Goebel, R., Schiltz, C., Rossion, B., 2007. Understanding the functional neuroanatomy of acquired prosopagnosia. Neuroimage 35, 836–852. https://doi.org/10.1016/j.neuroimage.2006.09.051

Steeves, J.K.E., Culham, J.C., Duchaine, B.C., Pratesi, C.C., Valyear, K.F., Schindler, I., Humphrey, G.K., Milner, A.D., Goodale, M.A., 2006. The fusiform face area is not sufficient for face recognition: Evidence from a patient with dense prosopagnosia and no occipital face area. Neuropsychologia 44, 594–609. https://doi.org/10.1016/j.neuropsychologia.2005.06.013

Stigliani, A., Weiner, K.S., Grill-Spector, K., 2015. Temporal Processing Capacity in High-Level Visual Cortex Is Domain Specific. J. Neurosci. 35, 12412–12424. https://doi.org/10.1523/JNEUROSCI.4822-14.2015

Striem-Amit, E., Dakwar, O., Reich, L., Amedi, A., 2012. The large-scale organization of "visual" streams emerges without visual experience. Cereb. Cortex 22, 1698–1709. https://doi.org/10.1093/cercor/bhr253

Susilo, T., Yang, H., Potter, Z., Robbins, R., Duchaine, B., 2015. Normal Body Perception despite the Loss of Right Fusiform Gyrus. J. Cogn. Neurosci. 27, 614–622.

Talairach, J., Tournoux, P., 1988. Co-planar Stereotaxic Atlas of the Human Brain.

Tootell, R.B., Mendola, J.D., Hadjikhani, N.K., Ledden, P.J., Liu, A.K., Reppas, J.B., Sereno, M.I., Dale, A.M., 1997. Functional analysis of V3A and related areas in human visual cortex. J. Neurosci. 17, 7060–78.

Vakli, P., Deák-Meszlényi, R.J., Hermann, P., Vidnyánszky, Z., 2018. Transfer learning

improves resting-state functional connectivity pattern analysis using convolutional neural networks. Gigascience 7. https://doi.org/10.1093/gigascience/giy130

van den Hurk, J., Van Baelen, M., Op de Beeck, H.P., 2017. Development of visual category selectivity in ventral visual cortex does not require visual experience. Proc. Natl. Acad. Sci. 114, E4501–E4510. https://doi.org/10.1073/pnas.1612862114

Wandell, B.A., Brewer, A.A., Dougherty, R.F., 2005. Visual field map clusters in human cortex. Philos. Trans. R. Soc. Lond. B. Biol. Sci. 360, 693–707. https://doi.org/10.1098/rstb.2005.1628

Wandell, B.A., Winawer, J., 2011. Imaging retinotopic maps in the human brain. Vision Res. 51, 718–737.

Wang, L., Mruczek, R.E.B., Arcaro, M.J., Kastner, S., 2014. Probabilistic Maps of Visual Topography in Human Cortex. Cereb. Cortex 1–21.

Weiner, K.S., Barnett, M.A., Witthoft, N., Golarai, G., Stigliani, A., Kay, K.N., Gomez, J., Natu, V.S., Amunts, K., Zilles, K., Grill-Spector, K., 2018. Defining the most probable location of the parahippocampal place area using cortex-based alignment and cross-validation. Neuroimage 170, 373–384. https://doi.org/10.1016/j.neuroimage.2017.04.040

Weiner, K.S., Golarai, G., Caspers, J., Chuapoco, M.R., Mohlberg, H., Zilles, K., Amunts, K., Grill-Spector, K., 2014. The mid-fusiform sulcus: a landmark identifying both cytoarchitectonic and functional divisions of human ventral temporal cortex. Neuroimage 84, 453–465. https://doi.org/10.1016/j.neuroimage.2013.08.068

Weiner, K.S., Grill-Spector, K., 2013. Neural representations of faces and limbs neighbor in human high-level visual cortex: Evidence for a new organization principle. Psychol. Res. 77, 74–97. https://doi.org/10.1007/s00426-011-0392-x

Weiner, K.S., Grill-Spector, K., 2011. Not one extrastriate body area: Using anatomical landmarks, hMT+, and visual field maps to parcellate limb-selective activations in human lateral occipitotemporal cortex. Neuroimage 56, 2183–2199. https://doi.org/10.1016/j.neuroimage.2011.03.041

Witthoft, N., Nguyen, M., Golarai, G., LaRocque, K.F., Liberman, A., Smith, M.E., Grill-Spector, K., 2014. Where is human V4? Predicting the location of hV4 and VO1 from

cortical folding. Cereb. Cortex 24, 2401–2408. https://doi.org/10.1093/cercor/bht092

Zeki, S., Kennard, C., Watson, J.D.G., Lueck, C.J., Frackowiak, R.S.J., 1991. Cortex of Functional Specialization in Human Visual 17.

Zimmermann, J., Goebel, R., de Martino, F., van de Moortele, P.F., Feinberg, D., Adriany, G., Chaimow, D., Shmuel, A., Uğurbil, K., Yacoub, E., 2011. Mapping the organization of axis of motion selective features in human area mt using high-field fmri. PLoS One 6, 1–10. https://doi.org/10.1371/journal.pone.0028716